27

Birth of a Magnetosphere

Hans Nilsson[1,2], Etienne Behar[1,2], James L. Burch[3], Christopher M. Carr[4], Anders I. Eriksson[5], Karl-Heinz Glassmeier[6], Pierre Henri[7], Marina Galand[4], Charlotte Goetz[6], Herbert Gunell[8,9], and Tomas Karlsson[10]

ABSTRACT

A magnetosphere may form around an object in a stellar wind either due to the intrinsic magnetic field of the object or stellar wind interaction with the ionosphere of the object. Comets represent the most variable magnetospheres in our solar system, and through the Rosetta mission we have had the chance to study the birth and evolution of a comet magnetosphere as the comet nucleus approached the Sun. We review the birth of the comet magnetosphere as observed at comet 67P Churyumov–Gerasimenko, the formation of plasma boundaries and how the solar wind–atmosphere interaction changes character as the cometary gas cloud and magnetosphere grow in size. Mass loading of the solar wind leads to an asymmetric deflection of the solar wind for low outgassing rates. With increasing activity a solar wind ion cavity forms. Intermittent shock-like features were also observed. For intermediate outgassing rate a diamagnetic cavity is formed inside the solar wind ion cavity, thus well separated from the solar wind. The cometary plasma was typically very structured and variable. The region of the coma dense enough to have significant collisions forms a special region with different ion chemistry and plasma dynamics as compared to the outer collision-free region.

27.1. INTRODUCTION

Comets are small bodies of the solar system with typically very elliptical orbits. Having formed in the far outer reaches of the solar system, the Kuiper belt or Oort cloud, they carry a large inventory of volatile gases and dust. These bodies become comets when their orbits are perturbed and they travel closer to the Sun. As the comet nucleus approaches the Sun its temperature increases and it begins to release volatile gases and dust, which can be seen as cometary tails. The volatile gases form a gas cloud not gravitationally bound by the small nucleus, called a coma. The ionized part of the coma interacts with the solar wind, and observations of cometary tails gave the first indications of the existence of a solar wind (Biermann, 1951). Alfvén (1957) provided a first theory on how a solar wind with a "frozen-in" magnetic field

[1]*Swedish Institute of Space Physics, Kiruna, Sweden*

[2]*Department of Computer Science, Electrical and Space Engineering, Luleå University of Technology, Kiruna, Sweden*

[3]*Southwest Research Institute, San Antonio, TX, USA*

[4]*Department of Physics, Imperial College London, London, UK*

[5]*Swedish Institute of Space Physics, Ångström Laboratory, Uppsala, Sweden*

[6]*Institut für Geophysik und extraterrestrische Physik, Technische Universität Braunschweig, Braunschweig, Germany*

[7]*Laboratoire de Physique et Chimie de l'Environnement et de l'Espace, UMR 7328 CNRS – Université d'Orléans, Orléans, France*

[8]*Royal Belgian Institute for Space Aeronomy, Brussels, Belgium*

[9]*Department of Physics, Umeå University, Umeå, Sweden*

[10]*Department of Space and Plasma Physics, School of Electrical Engineering and Computer Science, KTH Royal Institute of Technology, Stockholm, Sweden*

Space Physics and Aeronomy Collection Volume 2: Magnetospheres in the Solar System, Geophysical Monograph 259, First Edition.
Edited by Romain Maggiolo, Nicolas André, Hiroshi Hasegawa, and Daniel T. Welling.

DOI: 10.1002/9781119815624.ch27

would lead to field-line draping around the comet ionosphere.

In situ observations opened up the next big step in understanding solar wind interaction with the comet environment. The first space probe to observe a comet environment was the ICE spacecraft, which crossed the tail of comet 21P Giacobini–Zinner at a distance of 7,862 km while the comet was at a heliocentric distance of 1.03 astronomical units (au). It was followed by the "Halley armada," which encountered comet 1P Halley in 1986, at heliocentric distances between 0.79 and 0.89 au, with the closest approach being that of the Giotto spacecraft at 605 km from the nucleus (Cravens and Gombosi, 2004). Later cometary encounters, which included plasma measurements, were the Giotto extended mission to comet 26P/Grigg–Skjellerup (Johnstone et al., 1993) and the Deep Space 1 encounter with comet 19P/Borrelly (Young et al., 2004). All these encounters were relatively close to the Sun and thus had quite high outgassing rates.

The Rosetta mission (Glassmeier et al., 2007; Taylor et al., 2017) opened up the possibility to observe the birth and subsequent evolution of a comet magnetosphere, by following comet 67P/Churyumov–Gerasimenko from low outgassing rate (activity) at 3.6 au to moderate activity around perihelion at 1.24 au and out again. Rosetta carried a suite of plasma instruments to study the solar wind interaction with the coma, the Rosetta Plasma Consortium (RPC) (Carr et al., 2007). The RPC was made up of the Ion and Electron Sensor (IES) (Burch et al., 2007), the Ion Composition Analyzer (ICA) (Nilsson et al., 2007), the Langmuir probe (LAP) (Eriksson et al., 2007), the Mutual Impedance Probe (MIP) (Trotignon et al., 2007) and the Magnetic field experiment (MAG) (Glassmeier et al., 2007). The RPC instruments found the first unambiguous traces of the comet ionosphere during the first approach of Rosetta, water ions, at a heliocentric distance of 3.6 au and a comet nucleus distance of about 100 km (Nilsson et al., 2015a). A rich and unique data set was obtained during the two-year escort phase, until the very end of the mission, which offered the first density profile almost down to the surface during very low activity (Heritier et al., 2017).

What the Rosetta results clearly showed was that the size of the region where the cometary ion density affects the solar wind matters for comet–solar wind interaction. The size is essentially determined by the outgassing rate of the comet, which in turn is a property of each comet nucleus, but also a strong function of the distance to the Sun. The size of the comet–solar wind interaction region is further determined by the ionization rate, which also increases closer to the Sun. The outgassing rate (activity) of comet 67P during the Rosetta mission has been estimated from a number of measurements, primarily the local neutral density obtained with the Rosina COPS instrument (Balsiger et al., 2007). The activity of comet 67P during the active part of the Rosetta mission ranged from a few times 10^{25} s^{-1} during the end of mission, to 3.5 $\times 10^{28}$ s^{-1} around perihelion (Hansen et al., 2016). The largest of the comet magnetospheres encountered was that of comet 1P/Halley (outgassing rate 10^{30} s^{-1}) (Krankowsky et al., 1986; Rème, 1991); the bow shock was encountered at a distance of more than 1 million km, corresponding to an estimated stand-off distance at the subsolar point of 0.4 million km (Cravens and Gombosi, 2004). The bow shock was broad and weak, extending over ~100,000 km. For the least active comet encountered before Rosetta, 26P Grigg–Skjellerup, the bow shock was observed at about 20,000 km from the nucleus (Johnstone et al., 1993). Whereas the magnetosphere of comet 1P was much larger than a pickup ion gyroradius, that of 26P was of the same order. Johnstone et al. (1993) noted that the boundaries encountered still resembled those observed at comet 1P. In the rest of this chapter we look at how fundamentally the solar wind interaction with a coma changes when we go to the even smaller size represented by comet 67P during periods of low activity and a relatively weaker solar wind far from the Sun (section 27.4) and to a medium activity close to perihelion (section 27.5).

The main boundaries reported at an active comet (Halley) were the bow shock and the contact surface, separating the region of mass loading upstream of the bow shock, a cometosheath between the bow shock and the contact surface, and a diamagnetic cavity between the contact surface and the nucleus. In addition a few more tentative boundaries or regions were reported, e.g. a cometopause, an ion pile up boundary, and a magnetic field pileup boundary. A review of the boundaries observed at Halley in the context of Rosetta is given in Mandt et al. (2016).

27.2. OVERVIEW OF ROSETTA PLASMA OBSERVATIONS

Figure 27.1 shows an all-mission overview of the RPC observations. Upon arrival at the comet the few particles detected by ion spectrometers behaved as test particles (Nilsson et al., 2015a), moving along the solar wind electric field. As activity increased the cometary ions began to move more consistently antisunward and gradually attained higher energy (Nilsson et al., 2017). At the same time the magnetic field gradually increased in strength (Goetz et al., 2017). Around perihelion, the cometary ion distributions are less extended towards high energy (Mandt et al., 2016; Nilsson et al., 2017), as seen in Figure 27.1d. The solar wind deflection gradually increased with decreasing heliocentric distance (Figure 27.1e), without much energy loss (Behar et al., 2017). From June to

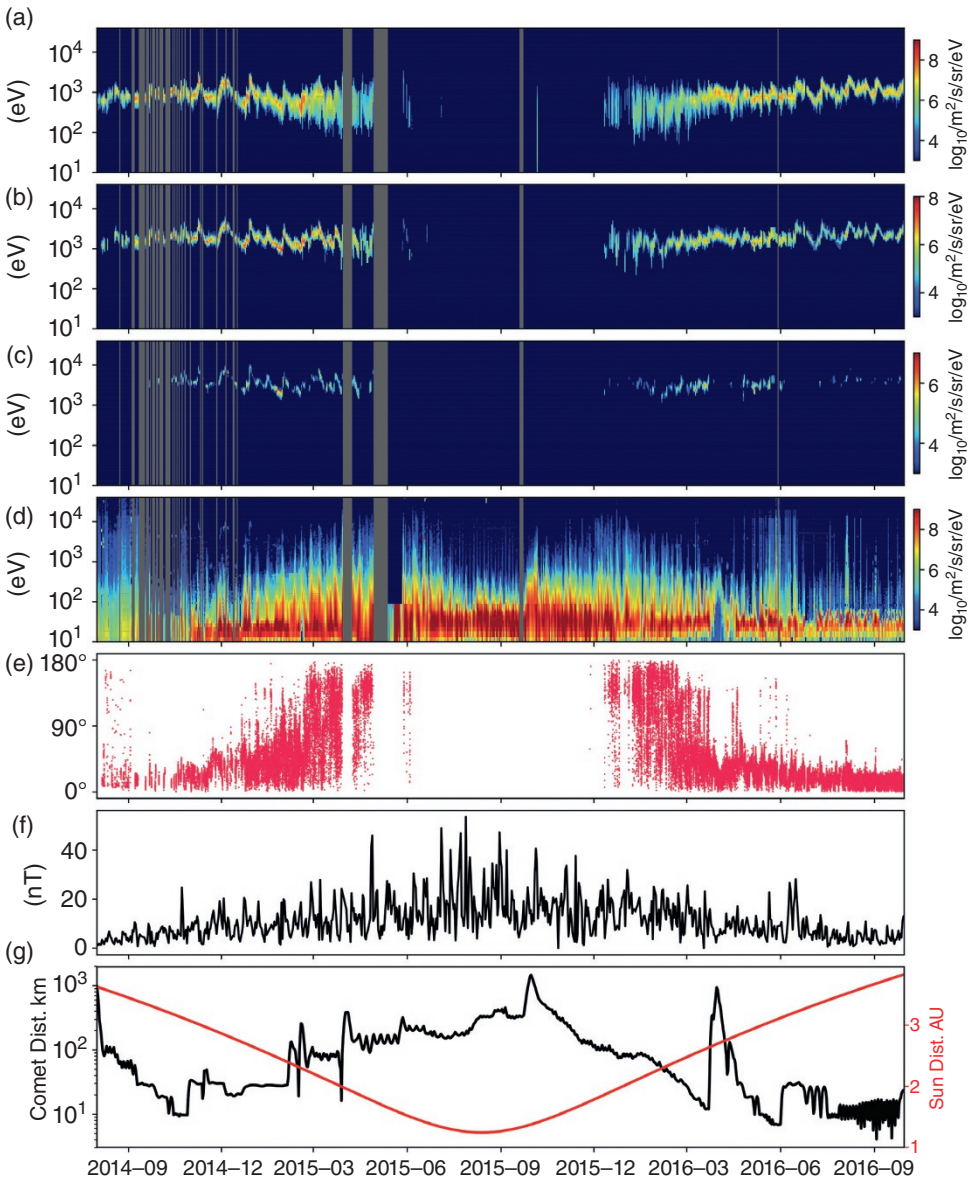

Figure 27.1 Data from the active part of the Rosetta mission, from arrival at the comet in August 2014 until end of mission in September 2016. Panels (a)–(d) show differential energy flux as function of energy (y-axis) and time (x-axis) for (a) H^+, (b) He^{2+}, (c) He^+, (d) cometary ions with a mass corresponding to water ions and above. Gray shading indicates data gaps. Panel (e) shows the solar wind deflection. Panel (f) shows the magnitude of the magnetic field averaged over 24 hours. Panel (g) shows the distance to the nucleus (black line, left y-axis) and heliocentric distance (red line, right y-axis).

November 2015 the solar wind ions were very rarely observed. In the 24-hour averaged energy spectra shown in Figure 27.1a, a broadening of the proton spectra can be seen just before the disappearance of the solar wind ions. This corresponds both to a larger variability and to some true broadening of the energy spectra. The He^{2+} ions showed less variability and broadening than the protons. Other ions were seen as well; the He^+ ions result from charge exchange between the He^{2+} ions and the coma (Nilsson et al., 2015a; Simon Wedlund et al., 2016). Even H^- ions were observed at solar wind energy (Burch et al., 2015).

The electron data show the presence of suprathermal electrons that appear to result from the solar wind–comet ionosphere interaction (Clark et al., 2015; Deca et al., 2017). The electrons may also be heated by lower hybrid waves (Broiles et al., 2016; Karlsson et al., 2017) or by the ambipolar electric field associated with the large scale

electron density gradient (Madanian et al., 2016). The magnetic field strength at the comet approximately followed the activity, increasing as the comet approached the Sun and then decreasing again after perihelion, reaching average daily values up to nearly 50 nT, with a highest instantaneous value of nearly 300 nT during one extreme event on 3 July 2015 (Goetz et al., 2019). The magnetic field magnitude was not stable, and variability increased with both increased cometary activity and solar wind activity, as seen by other impulsive solar wind pressure events such as ICMEs (Edberg et al., 2016a) and CIRs (Edberg et al., 2016b; Hajra et al., 2018a). On top of the magnetic and cometary plasma variability controlled by the solar wind dynamics, impulsive cometary outburst were also observed to account for the cometary induced magnetosphere variability (Grün et al., 2016; Hajra et al., 2017).

Rosetta sampled a very limited region of the comet magnetosphere, namely the portion of the plane perpendicular to the Sun–comet direction within a few hundred km from the nucleus, beside two larger excursions, one dayside, i.e. on the sunward side of the comet (Edberg et al., 2016a), and one nightside, further away from the Sun than the nucleus (Behar et al., 2018a). The dayside excursion took place inside the magnetosphere while the nightside excursion occurred during low activity when the solar wind permeated all the region sampled by Rosetta. The dayside and nightside excursions can readily be identified in Figure 27.1g as the two highest peaks in cometary distance (black line, left-hand scale). The dayside excursion showed that this close to perihelion the bow shock and any possible cometosheath with shocked solar wind plasma was further away from the nucleus than 1,500 km, though some weak fluxes of solar wind origin ions were seen in conjunction with a coronal mass ejection (Edberg et al., 2016a). The nightside excursion offered an unprecedented possibility both to study the root of a cometary tail and to verify models of mass loading and solar wind deflection over larger distances. We show a comparison of the solar wind flow direction as observed during the nightside excursion and according to a simple mass-loading model in Figure 27.2 (Behar et al., 2018a).

27.3. ELECTRIC FIELDS IN A COMET MAGNETOSPHERE

Because the ion environment of comet 67P was typically much smaller than a pickup ion gyroradius, the cometary ions tended to move along the electric fields present. Figure 27.3 shows the observed effect of three different electric fields in the ion data. Ions accelerated several tens of eV were mainly accelerated antisunward, while their motion in the plane perpendicular to the sun-line (the Y-Z plane in CSEQ, CSO, and CSE reference frames) was determined by the direction of the solar wind electric field. Ions at lower energy had their flow direction in the Y-Z plane away from the nucleus irrespective of the direction of the solar wind electric field. The latter indicates that for the more locally produced ions an ambipolar electric field is also important. During the whole nightside excursion the cometary ion flow was close to radially away from the nucleus, also irrespective of the direction of the solar wind electric field (Behar et al., 2018a).

It has been suggested that the antisunward acceleration is due to a polarization electric field arising due to the different response of cometary ions and electrons to the imposed solar wind electric field (Nilsson et al., 2015b, 2017; Behar et al., 2016; Berčič et al., 2018). The ions would move along the solar wind electric field, but the electrons of the cometary ionosphere would, assuming the electron gyroradius is small compared to the comet environment, move with the $E \times B$ drift. Ions and electrons cannot separate significantly before a polarization electric field builds up. The different motion of ions and electrons give rise to an ion and an electron current, which buildup charges at the boundary of the comet ionosphere. These charges propagate outward as a field-aligned current. A steady-state solution can be found where the different currents balance each other. This scenario was investigated by Nilsson et al. (2018), using a model by Brenning et al. (1991) developed to describe barium cloud releases. The polarization electric field will partly or wholly cancel the solar wind electric field in the denser part of the comet ionosphere. In the case of partial cancellation it was shown by Nilsson et al. (2018) that the polarization electric field could account for the observed antisunward acceleration of cometary ions. Particle-in-cell simulations by Deca et al. (2017) show how this field also affects the electrons, resulting in a pattern where solar wind electrons neutralize cometary ions while the cometary origin electrons neutralize the solar wind ions. Apart from the polarization electric field, which can develop at the boundaries of a dense cometary ion cloud (i.e., the inner part of a comet ionosphere, where the cometary ion density dominates), mass loading will also slow down the electron plasma into which the magnetic field is frozen in, as the electrons cannot move independently of the slow cometary ions (Behar et al., 2018b). This is also seen in the pileup of the magnetic field (Goetz et al., 2017).

27.4. BEFORE THE BOUNDARIES FORM

27.4.1. Mass Loading

Mass loading is the process of gradually adding new plasma to the solar wind stream (Szegö et al., 2000).

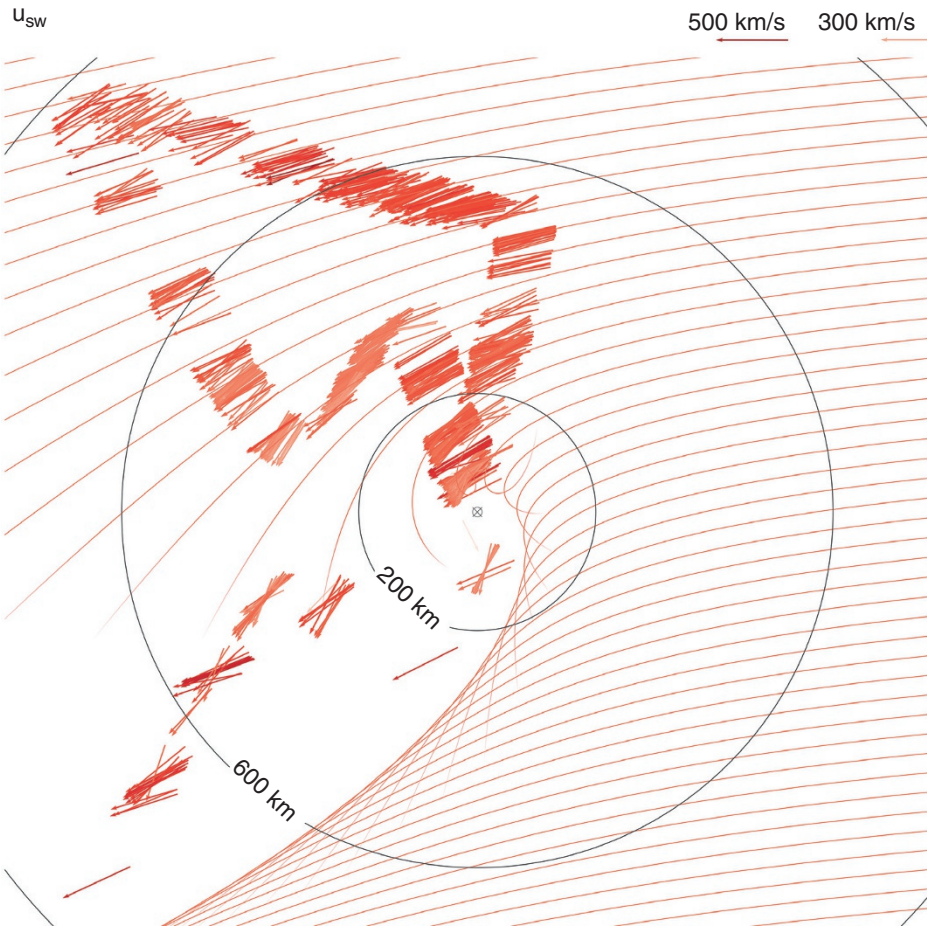

Figure 27.2 Observed solar wind proton flow during the nightside excursion (red arrows). The excursion took place between 23 March and 8 April 2016, at a heliocentric distance of 2.7 au. Corresponding flow lines of the solar wind protons obtained from a mass-loading model are shown as red lines. The undisturbed solar wind electric field is directed upward in the figure. The Sun is to the right. In the lower part of the figure it can be seen how solar wind flow trajectories converge in a limited region, which we term a caustic in analogy with light rays. A region free of solar wind ions can also be seen around the nucleus, the solar wind ion cavity. To the right in the figure one can see the gradual deflection of the solar wind acting over large distances. Adapted from Behar et al. (2018a). Licensed under CC BY 4.0.

A small fraction of the coma is ionized, mainly due to solar EUV radiation but also due to electron impact ionization and charge exchange collisions (Galand et al., 2016; Simon Wedlund et al., 2017). Electron impact was shown to be the most important factor at large heliocentric distances, especially post perihelion, whereas EUV ionization dominated close to perihelion (i.e., when Rosetta was located in the inner part of the magnetosphere) (Heritier et al., 2018). As the coma is expanding into the surrounding space, and only a small fraction is ionized, the process will also be ongoing outside any plasma boundary formation. For a comet magnetosphere gradually taking shape, being born, the first significant signature is a deflection of the solar wind. This deflection can be interpreted as a conservation of momentum. Cometary ions are accelerated along the direction of the solar wind electric field, and the solar wind is deflected in the opposite direction. Behar et al. (2018b) described this in a more complete manner as a generalized gyromotion of two plasma streams. The solar wind ions can be seen as gyrating in the slowed-down net plasma drift, that of a slowed-down electron fluid, which is indicated also by the pileup of the magnetic field frozen into the electron fluid. The motional electric field is then not only given by the solar wind but by the average ion velocity. At the lower outgassing rates typical for Rosetta observations outside the boundaries, no clear field-line draping could be discerned (Goetz et al., 2017), except close to the nucleus. Koenders et al. (2016a) showed how close to the nucleus (less than 50 km from the nucleus and

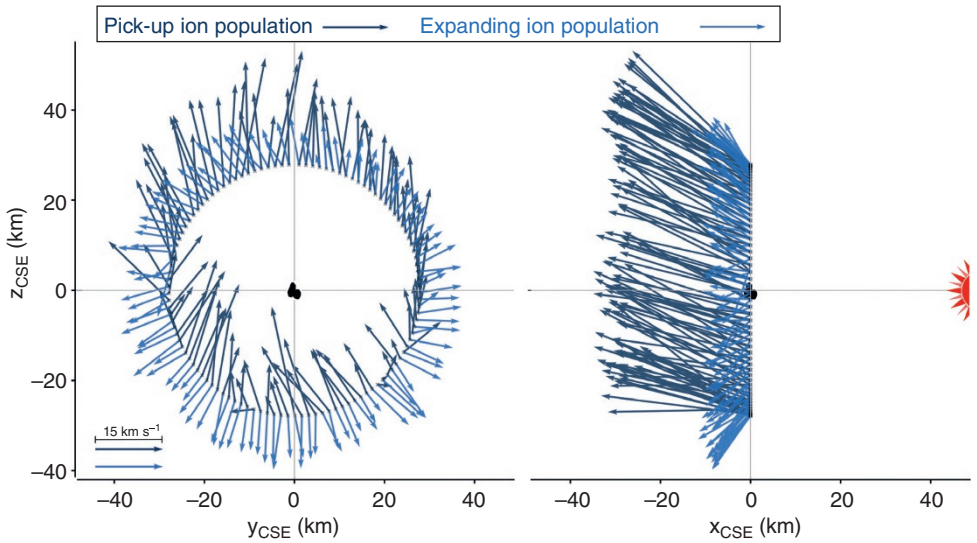

Figure 27.3 Velocity vectors of the pickup and expanding cometary ion populations, indicated in different colors. Two planes are shown in the CSE frame: on the left the terminator plane (Y-Z plane) and on the right the X-Z plane. From Berčič et al. (2018). Licensed under CC BY 4.0.

2.0 au from the Sun) a draping almost perpendicular to the original solar wind flow direction was observed, consistent with draping from a strongly deflected solar wind. The field-line draping expected due to the mass loading could be observed for high enough activity (Goetz et al., 2017), including nested draping (layers of oppositely directed draped magnetic field lines) due to changing upstream solar wind magnetic field direction (Volwerk et al., 2017). During the tail excursion (at 2.7 au heliocentric distance) no draping was seen (Volwerk et al., 2018).

The more cometary plasma that is present, the more deflected the solar wind will be. In a simple mass-loading model the integrated effect is a concentration of the solar wind towards the negative flank of the comet in the CSE reference frame (Behar et al., 2016, 2018b), which in accordance with similar phenomena for light has been termed a "caustic". The plasma environment at low activity is fundamentally asymmetric. Furthermore the deflection of the solar wind in a model only taking mass loading into account predicts the formation of a solar wind ion cavity. The caustic and solar wind ion cavity as they appear in the model of Behar et al. (2018b) are shown in Figure 27.2. Note that what is shown is individual ion trajectories, not flow lines. Thus several of the main boundary phenomena expected and observed at a comet would form through just the gradual deflection of solar wind ions over the full region affected by mass loading. The real physical processes when the boundaries do form are more complex, as discussed in section 27.5, but the gradual mass loading sets the stage by having already affected the flow of the solar wind incident on the forming boundaries.

The detailed effect of mass loading at comet 67P was best highlighted by the gradual change of the observed solar wind deflection with activity (Behar et al., 2017) and by the solar wind flow during the nightside excursion (Behar et al., 2018a). Most striking in the former observation was a concentrated flow of solar wind ions with a deflection of about 140° in the time just before and after Rosetta spent a long time in the solar wind ion cavity, as shown in Figure 27.1e. Both show a very good agreement with the simple mass-loading model of Behar et al. (2018b), which is shown in Figure 27.2 for the low activity conditions during the nightside excursion. Another effect of mass loading is a consistent dusk to dawn flow of cometary ions, with the solar wind deflected in the opposite directions, as predicted by the mass-loading model and as observed at comet 67P (Behar et al., 2018).

Also in a rather tenuous coma, the solar wind is affected by charge-changing reactions, either electron capture or stripping reactions. These collisions remove solar wind ions and add slow cometary ions (Simon Wedlund et al., 2019a, 2019b, 2019c). A decrease in solar wind density can thus occur due to charge exchange, which will also affect the mass loading and lead to a modulation of the size of cometary plasma boundaries (Simon Wedlund et al., 2019b). As electron capture is in general not offset by stripping of the energetic neutral atoms, essentially all of the solar wind ions can be turned into neutrals (Simon Wedlund et al., 2019c).

The integrated effect of charge exchange on He^{2+} ions can be seen in the presence of He+ ions, (Figures 27.1b and 27.1c).

27.4.2. Wave Environment

During the period when the solar wind permeated the entire (or most of) the coma, the most prominent waves were the so called "singing comet waves" (Richter et al., 2015). These are large amplitude oscillations of the magnetic field, also seen in hybrid simulations (Koenders et al., 2016b). A suggested source of these waves is a modified ion-Weibel instability, resulting from the current generated by essentially unmagnetized cometary ions (due to their large gyroradius), as described by Meier et al. (2016). In the regions outside the boundaries, or before they formed, ion acoustic waves have also been reported (Gunell et al., 2017a). Cyclotron waves, as observed at the larger comets (Glassmeier et al., 1989), were not observed at comet 67P. At comet Grigg–Skjellerup, which was more similar to Churyumov–Gerasimenko close to perihelion, strong cyclotron waves were observed (Neubauer et al., 1993; Glassmeier and Neubauer, 1993), where it was suggested that nongyrotropic ring distributions, caused by the small scale of the system compared to the ion gyroradius, could lead to enhanced cyclotron wave generation (Motschmann and Glassmeier, 1993). Apparently, once the system gets small enough, no cyclotron waves are observed, nor any full ring distributions of cometary ions, at least at the distances probed by Rosetta.

27.5. EMERGENCE OF BOUNDARIES

27.5.1. Solar Wind Ion Cavity and Shocks

In section 27.4 we described how the solar wind was affected by mass loading alone, outside or before boundary formation. One of the clearest boundaries to emerge at sufficient activity was a solar wind ion cavity, observed in the RPC-ICA and RPC-IES data (Behar et al., 2017; Nilsson et al., 2017; Mandt et al., 2016), with the solar wind starting to disappear in May 2015 and reappearing again in December 2015. In the time period before Rosetta entered the solar wind ion cavity, the most common observation was that of a solar wind deflected about 140° and little loss of energy or broadening of the proton energy spectra. Clear partial ring distribution of solar wind protons were observed. This indicates that the region just outside of the solar wind cavity is dominated by a slowed down electron fluid with gyrating protons, i.e. the mass-loading region.

As activity increased, broadened proton spectra appeared sporadically (Nilsson et al., 2015b). Broadening of the proton spectra may result from shocks within the solar wind (Hajra et al., 2018a), but this does not explain them being more common close to the solar wind ion cavity. The broadened proton energy spectra were studied by Gunell et al. (2018) who found that there was also a clear increase in the magnetic field amplitude and electron heating associated with the investigated events. They also showed how this was in agreement with the FLASH hybrid model, which predicted a rather small region of heated solar wind plasma with no clear magnetosheath for intermediate activity (Lindkvist et al., 2018). This can then explain why such observations of broadened proton spectra were less common than the region with mass-loaded plasma and gyrating solar wind ions just before Rosetta entered the solar wind ion cavity, i.e., due to the size difference of the two regions. Lindkvist et al. (2018) used the FLASH hybrid model to see how energy was transferred between plasma and electromagnetic fields in the model (i.e., generator and loads). The model showed a shock-like structure similar in form and position as the caustic predicted by mass loading, and that this region acted as a generator, transferring energy from the plasma to the electromagnetic fields. This is consistent with the physics in this region moving from the simple mass-loading picture to one where the full self-consistent interaction between plasma and fields must be taken into account. A similar structure, a bow wave, was reported by Bagdonat and Motschmann (2002), who noted that in their model the bow wave was adiabatic and not a shock. Rosetta was mostly located within a region characterized by the simple mass-loading picture, and where the change occurs is a function of the heliocentric distance and outgassing rate. Behar et al. (2018b) made a direct comparison of a simple model of mass loading and results using the FLASH hybrid code and showed how the caustic and solar wind ion cavity were closely colocated for the two models. Nilsson et al. (2018) noted that the shape of the cometary ion energy spectra observed could constitute the remote detection of a larger scale bow shock, tentatively located at about 4,000 km upstream of the observation point, an interpretation later supported by hybrid simulations (Alho et al., 2019).

Early work on mass loading indicated that the solar wind flow can be slowed by mass loading, but only up to some point, where a shock must form. Biermann et al. (1967) and Flammer and Mendis (1991) showed this in the simplest form using 1-D models: the shock would occur when the mass-loaded ion flux normalized to the upstream value reached a critical value. MHD simulations and observations from more active comets showed the presence of a shock (Huang et al., 2016; Ogino et al., 1988), which occurs at a relative cometary ion particle density of a few percentage relative to the solar wind. Almost all Rosetta observations were obtained when the

cometary ions already by far dominated the particle density, typically being above 10 cm^{-3} since the first observations (Nilsson et al., 2015a) and then reaching up to several 1,000 cm^{-3} in regions outside the solar wind ion cavity. The situation at the low to intermediate activity comet is thus very different from that of a larger scale more active comet.

27.5.2. Ion-Neutral and Electron-Neutral Collisionopause

The next boundary reported was the ion-neutral collisionopause or ion exobase (Mandt et al., 2016). Higher energy cometary ions were seen outside the boundary, while low-energy cometary ions along with reduced magnetic field pileup and enhanced electron densities were seen inside the boundary. The boundary may be related to the ion-neutral collision rate. Studies of Langmuir probe data, however, revealed that the ions at the location of Rosetta appeared to be not collisionally coupled to the neutrals (Odelstad et al., 2018a; Vigren and Eriksson, 2017). It still seems clear that a boundary exists separating a region where collisions matter, both for the bulk velocities of ions and for the role of ion chemistry producing H_3O^+ and other ions (Fuselier et al., 2016; Beth et al., 2017). Models of the plasma density also indicate that when Rosetta was close enough to the comet the ions were moving with a similar speed to that of the neutrals (Galand et al., 2016; Heritier et al., 2017). The tentative collisionopause boundary was identified in RPC-IES data intermittently from April 2015 to January 2016, i.e., essentially throughout the period when the solar wind ion cavity was detected by Rosetta. Another, not necessarily conflicting, explanation for lower energy of accelerated cometary ions during the period of high activity around perihelion was given by Nilsson et al. (2018). They showed how the solar wind electric field could be more efficiently shielded during this time period, which would lead to lower energies of the ions. Using a simple cloud model, they found that the net electric field was typically less than 0.1 mV m^{-1} around perihelion, while a few times 0.1 mV^{-1} was typical for larger heliocentric distances.

Even closer to the nucleus, a region dominated by electron-neutral collision, within a so-called electron exobase, has been inferred by the observation of cold electrons (Eriksson et al., 2017; Gilet et al., 2017; Engelhardt et al., 2018a). An estimate of the position of the electron exobase, i.e. the region inside which electron-neutral collisions are expected to be significant, was given in Mandt et al. (2016) for the period April to September 2015, typically being within a few tens of kilometers from the nucleus, reaching up to about 250 km from the nucleus in the beginning of September. These electrons, cooled by collisions on the cometary neutral atmosphere (Vigren and Galand, 2013), contrast with the fairly warm electrons typically observed at the location of Rosetta, as evidenced by both electron observations and a negative spacecraft potential (Broiles et al., 2016; Goldstein et al., 2017; Odelstad et al., 2015, 2017) during most of the mission. Eriksson et al. (2017) and Engelhardt et al. (2018a) showed how filaments of cold electron plasma were detected at the location of Rosetta, seen as by intermittent pulses of high probe current of a few to a few tens of seconds in duration, also well outside the electron exobase. By combining LAP and MIP data, (Engelhardt et al., 2018a) could show that cold electrons (order 0.1 eV) indeed are commonly seen by Rosetta, starting at about 3 au heliocentric distance and increasing in frequency until being seen almost always around perihelion.

27.5.3. Diamagnetic Cavity

Another boundary forming (mostly) within the solar wind ion cavity is the diamagnetic cavity, a region free not only of the solar wind ions but also of the interplanetary magnetic field carried by the solar wind. The first diamagnetic cavity reported at comet 67P was seen at the end of July 2015 (Goetz et al., 2016a), at a distance of 170 km from the nucleus. This was much further from the nucleus for the prevailing gas production rate of 4×10^{27} s^{-1} than was expected based on the model of Cravens (1989), which had been used to explain the diamagnetic cavity observed at comet 1P/Halley (Neubauer et al., 1986). It was also further away than the diamagnetic cavity predicted by steady-state simulations (Koenders et al., 2015). Later studies showed that the diamagnetic cavity was observed intermittently from April 2015 to February 2016 (Goetz et al., 2016b), somewhat overlapping in time with periods outside the solar wind ion cavity. The many short observations of the diamagnetic cavity, often far from the nucleus, indicated a filamentary or otherwise unsteady diamagnetic cavity (Henri et al., 2017) rather than a large field-free region as envisioned for comet 1P/Halley.

The plasma inside the diamagnetic cavity was typically depleted of suprathermal electrons (Nemeth et al., 2016), rather uniform, and occurred close to the electron exobase (Henri et al., 2017). However, at times plasma density enhancements are seen inside the diamagnetic cavity (Hajra et al., 2018b). These structures look similar to structures observed outside the diamagnetic cavity and appear to have been transmitted from the magnetized region into the diamagnetic cavity. The plasma just outside the diamagnetic cavity is very structured, as is seen in the data from all RPC sensors. On a timescale of minutes, the plasma density can vary by an order of magnitude (Hajra et al., 2017; Engelhardt et al., 2018b), the ion energy by tens of eV, and their flux by a factor ten

(Stenberg Wieser et al., 2017), and the magnetic field strength by tens of nT (Goetz et al., 2016b), all well correlated (Odelstad et al., 2018a; Stenberg Wieser et al., 2017). Similar structures were predicted by the hybrid simulations of Koenders et al. (2015) to originate from the diamagnetic cavity boundary and propagate outward. No comparison of the statistical properties of observed and simulated structures have yet been done.

The observations and theories related to comet 1P/Halley indicated that the solar wind ions were present up to the diamagnetic cavity (Neugebauer, 1990). The observations around comet 67P clearly showed that the solar wind ion cavity and the diamagnetic cavity were separate features. Despite this, it has been shown that the position of the diamagnetic cavity around 67P statistically relates well to the position determined by a model invoking plasma-neutral drag as the outward force (Nemeth et al., 2016).

27.5.4. Wave Environment Inside the Boundaries

Gunell et al. (2017b) reported ion acoustic waves confined inside the diamagnetic cavity. The observations were interpreted as current-driven ion acoustic waves, generated by current that flows through bulges in the surface of the diamagnetic cavity. Just outside the diamagnetic cavity, high-amplitude density fluctuations in the electron density in a frequency range similar to the ion cyclotron frequency were seen Odelstad et al. (2018b). Further out in the comet magnetosphere, mirror mode waves have been observed Volwerk et al. (2016).

Strong wave activity around the lower hybrid frequency range was detected mainly inside the comet magnetosphere, as reported in Karlsson et al. (2017), André et al. (2017) and Stenberg Wieser et al. (2017). The wave activity was usually coincident with large density gradients, and it was shown that the necessary requirements for the lower hybrid drift instability were fulfilled (Karlsson et al., 2017). André et al. (2017) investigated the generation of lower hybrid waves in the cometary environment in more detail. The observed wave amplitudes could be quite high, tens of mV m^{-1}, indicating that these waves significantly affect the ion and electron environment. Madsen et al. (2017) showed wave activity in the 3–8 Hz range inside the diamagnetic cavity, which was interpreted as ion acoustic waves excited by "cavity boundary forcing" from the lower hybrid waves outside.

27.6. FUTURE DIRECTIONS

The changes Rosetta revealed as a comet magnetosphere is "born" are related to the increasing relative role of the cometary plasma and the increasing scale size of the interaction region. Comet 67P is indeed a mass-loading laboratory in this respect, allowing us to sample a gradually changing environment. The main drawback with the Rosetta observations is the lack of spatial coverage. Therefore, the data must be combined with 3-D models. At small cometocentric distances during periods of high activty near perihelion, these models need to take into account collisions with the neutral atmosphere. Electron dynamics and charge distribution are important, as evidenced by the role of the ambipolar electric field and possibly a polarization electric field arising from the different response of cometary ions and electrons to the imposed solar wind electric field. Mass loading has an integrated effect over large distances, so that large simulation boxes are needed for accurate results.

On a larger scale the transition from the mass-loaded regime to one where shocks start to occur – and matter – is important. In the mass-loaded plasma, the solar wind ions are seen to be gyrating, which can be regarded as the equivalent of a thermal motion in the sense that it is a motion in addition to the now much slower guiding center motion of the plasma, so what is observed shares some features to be expected downstream of a shock. At some point the solar wind ions start to lose more energy and obtain a more spread motion. A careful comparison of the response seen in H^+ and He^{2+} may give an indication of the role of the local ion gyroradius. All the different data sets must be combined in order to see the role of feedback between particles and fields.

For a future cometary mission, an energetic neutral atom (ENA) instrument would be a valuable addition. Comets produce significant amounts of ENA and observations of charge-exchanged solar wind could allow a remote sensing of upstream conditions. A second highly valuable addition to future cometary space missions would be the presence of a dedicated, separated solar wind spacecraft, able to monitor the solar wind state and variability upstream the solar wind–comet interaction region, in order to enable separating the intrinsic cometary magnetosphere dynamics to that directly induced by the solar wind variability.

ACKNOWLEDGMENTS

Rosetta is a European Space Agency (ESA) mission with contributions from its member states and the National Aeronautics and Space Administration (NASA). HN was supported by SNSA grants 95/15, 112/13, 108/12 and VR grant 2015-04187. MG was supported by STFC of UK under grant ST/N000692/1. This work benefitted from the International Space Science Institute (ISSI) support for project 2017-402. PH was supported by ESEP, CNES, and by ANR under the financial agreement ANR-15-CE31-0009-01. We acknowledge the

staff of CDDP and Imperial College London for the use of AMDA and the RPC Quicklook database (provided by a collaboration between the Centre de Donnees de la Physique des Plasmas, supported by CNRS, CNES, Observatoire de Paris and Universite Paul Sabatier, Toulouse, and Imperial College London, supported by the UK Science and Technology Facilities Council). RPC data is available through the ESA PSA site. We are indebted to the whole Rosetta mission team, Science Ground Segment and Rosetta Mission Operation Control for their hard work making this mission possible.

REFERENCES

Alfvén, H. (1957), On the theory of comet tails, *Tellus*, IX, 92.

Alho, M., C. Simon Wedlund, H. Nilsson, E. Kallio, R. Jarvinen, and T. Pulkkinen (2019), Hybrid modelling of cometary plasma environments. II. Remote sensing of a cometary bow shock, *Astron. Astrophys.*, 630, A45.

André, M., E. Odelstad, D. B. Graham, A. I. Eriksson, T. Karlsson, G. Stenberg Wieser, et al. (2017), Lower hybrid waves at comet 67P/Churyumov–Serasimenko, *Mon. Not. R. Astron. Soc.*, 469(Suppl2), S29–S38, doi:10.1093/mnras/stx868.

Bagdonat, T., and U. Motschmann (2002), From a weak to a strong comet – 3D global hybrid simulation studies, *Earth Moon, Planets*, 90, 305–321, doi:10.1023/A:1021578232282.

Balsiger, H., K. Altwegg, P. Bochsler, P. Eberhardt, J. Fischer, S. Graf, et al (2007), Rosina Rosetta orbiter spectrometer for ion and neutral analysis, *Space Sci. Rev.*, 128, 745–801, doi:10.1007/s11214-006-8335-3.

Behar, E., J. Lindkvist, H. Nilsson, M. Holmström, G. Stenberg-Wieser, R. Ramstad, and C. Götz (2016), Mass-loading of the solar wind at 67P/Churyumov-Gerasimenko. Observations and modelling, *Astron. Astrophys.*, 596, A42, doi:10.1051/0004-6361/201628797.

Behar, E., H. Nilsson, M. Alho, C. Goetz, C., and B. Tsurutani (2017), The birth and growth of a solar wind cavity around a comet – Rosetta observations, *Mon. Not. R. Astron. Soc.*, 469 (Suppl2), S396–S403.

Behar, E., H. Nilsson, P. Henri, L. Berčič, G. Nicolaou, G. Stenberg Wieser, et al.(2018a), The root of a comet tail: Rosetta ion observations at comet 67P/Churyumov-Gerasimenko, *Astron. Astrophys.*, 616, A21, doi:10.1051/0004-6361/201832842.

Behar, E., B. Tabone, M. Saillenfest, J. Deca, M. Holmström, and H. Nilsson (2018b), Solar wind dynamics around a comet – A 2D semi-analytical model, *Astron. Astrophys.*, 620, A35, doi:10.1051/0004–6361/201832,736, doi:10.1051/0004-6361/201832736.

Behar, E., B. Tabone, and H. Nilsson (2018), Dawn-dusk asymmetry induced by the Parker spiral angle in the plasma dynamics around comet 67P/Churyumov-Gerasimenko, *Mon. Not. R. Astron. Soc.*, 478(2), 1570–1575, doi:10.1093/mnras/sty1111.

Berčič, L., E. Behar, H. Nilsson, G. Nicolaou, G. Stenberg Wieser, M. Wieser, and C. Goetz (2018), Cometary ion dynamics observed in the close vicinity of comet 67P/CG, *Astron. Astrophys.*, 13, A57, doi:10.1051/0004–6361/201732082.

Beth, A., K. Altwegg, H. Balsiger, J.-J. Berthelier, U. Calmonte, M. R. Combi, et al. (2017), First in-situ detection of the cometary ammonium ion NH+ (protonated ammonia NH_4^+) in the coma of 67P/C-G near perihelion, *Mon. Not. R. Astron. Soc.*, doi:10.1093/mnras/stw3370.

Biermann, L. (1951), Kometenschweife under solar korpuskularstrahlung, *Zeitschrift fur Astrophysik*, 29, 274.

Biermann, L., B. Brosowski, and H. U. Schmidt (1967), The interaction of the solar wind with a comet, *Sol. Phys.*, 1(2), 254–284, doi:10.1007/BF00150860.

Brenning, N., M. C. Kelley, J. Providakes, H. C. Stenbaek-Nielsen, and C. Swenson (1991), Barium swarm – An ionospheric alternating current generator in CRIT I, *J. Geophys. Res.*, 96, 9735–9743, doi:10.1029/90JA01974.

Broiles, T. W., J. L. Burch, K. Chae, G. Clark, T. E. Cravens, A. Eriksson, et al. (2016), Statistical analysis of suprathermal electron drivers at 67P/Churyumov-Gerasimenko, *Mon. Not. R. Astron. Soc.*, 462, S312–S322, doi:10.1093/mnras/stw2942.

Burch, J., R. Goldstein, T. Cravens, W. Gibson, R. Lundin, C. Pollock, et al. (2007), RPC-IES: The ion and electron sensor of the rosetta plasma consortium, *Space Sci. Rev.*, 128(1-4), 697–712, doi:10.1007/s11214-006-9002-4.

Burch, J. L., T. E. Cravens, K. Llera, R. Goldstein, P. Mokashi, C.-Y. Tzou, and T. Broiles (2015), Charge exchange in cometary coma: Discovery of H^- ions in the solar wind close to comet 67P/Churyumov-Gerasimenko, *Geophys. Res. Lett.*, 42, 5125–5131, doi:10.1002/2015GL064504.

Carr, C., E. Cupido, C. G. Y. Lee, A. Balogh, T. Beek, J. L. Burch, et al. (2007), RPC The ROSETTA Plasma Consortium, *Space Sci Rev.*, 128(1-4), 629–647.

Clark, G., T. W. Broiles, J. L. Burch, G. A. Collinson, T. Cravens, R. A. Frahm, et al. (2015), Suprathermal electron environment of comet 67P/Churyumov-Gerasimenko: Observations from the Rosetta Ion and Electron Sensor, *Astron. Astrophys.*, 583, A24, doi:10.1051/0004-6361/201526351.

Cravens, T. E. (1989), A magnetohydrodynamical model of the inner coma of comet halley, *J. Geophys. Res.: Space Phys.*, 94 (A11), 15,025–15,040, doi:10.1029/JA094iA11p15025.

Cravens, T., and T. Gombosi (2004), Cometary magnetospheres: a tutorial, *Adv. Space Res.*, 33(11), 1968–1976, http://dx.doi.org/10.1016/j.asr.2003.07.053.

Deca, J., A. Divin, P. Henri, A. Eriksson, S. Markidis, V. Olshevsky, and M. Horányi (2017), Electron and ion dynamics of the solar wind interaction with a weakly outgassing comet, *Phys. Rev. Lett.*, 118(20), 205101, doi:10.1103/PhysRevLett.118.205101.

Edberg, N. J. T., M. Alho, M. André, D. J. Andrews, E. Behar, J. L. Burch, et al. (2016a), CME impact on comet 67P/Churyumov-Gerasimenko, *Mon. Not. R. Astron. Soc.*, 462, S45–S56, doi:10.1093/mnras/stw2112.

Edberg, N. J. T., A. I. Eriksson, E. Odelstad, E. Vigren, D. J. Andrews, F. Johansson, et al. (2016b), Solar wind interaction with comet 67P: Impacts of corotating interaction regions, *J. Geophys. Res.: Space Phys.*, 121(2), 949–965, doi:10.1002/2015JA022147.

Engelhardt, I. A. D., A. I. Eriksson, E. Vigren, X. Valliéres, M. Rubin, N. Gilet, and P. Henri (2018a), Cold electrons at comet 67P/Churyumov-Gerasimenko, *Astron. Astrophys.*, 616, A51, doi:10.1051/0004-6361/201833251.

Engelhardt, I. A. D., A. I. Eriksson, G. Stenberg Wieser, C. Goetz, M. Rubin, P. Henri, et al. (2018b), Plasma density structures at comet 67p/Churyumov-Gerasimenko, *Mon. Not. R. Astron. Soc.*, 477(1), 1296–1307, doi:10.1093/mnras/sty765.

Eriksson, A. I., R. Boström, R. Gill, L. Åhlén, S.-E. Jansson, J.-E. Wahlund, et al. (2007), RPC-LAP: The Rosetta Langmuir Probe Instrument, *Space. Sci. Rev.*, 128, 729–744, doi:10.1007/s11214-006-9003-3.

Eriksson, A. I., I. A. D. Engelhardt, M. André, R. Boström, N. J. T. Edberg, F. L. Johansson, et al. (2017), Cold and warm electrons at comet 67P/Churyumov-Gerasimenko, *Astron. Astrophys.*, 605, A15, doi:10.1051/0004-6361/201630159.

Flammer, K. R., and D. A. Mendis (1991), A note on the mass-loaded MHD flow of solar wind towards a cometary nucleus, *Astrophys. Space Sci.*, 182(1), 155–162, doi:10.1007/BF00646450.

Fuselier, S. A., K. Altwegg, H. Balsiger, J. J. Berthelier, A. Beth, A. Bieler, et al. (2016), Ion chemistry in the coma of comet 67P near perihelion, *Month. Not. Roy. Astron. Soc.*, 462, S67–S77, doi:10.1093/mnras/stw2149.

Galand, M., K. L. Héritier, E. Odelstad, P. Henri, T. W. Broiles, A. J. Allen, et al. (2016), Ionospheric plasma of comet 67P probed by Rosetta at 3 au from the Sun, *Mon. Not. R. Astron. Soc.*, 462, S331–S351, doi:10.1093/mnras/stw2891.

Gilet, N., P. Henri, G. Wattieaux, M. Cilibrasi, and C. Béghin (2017), Electrostatic potential radiated by a pulsating charge in a two-electron temperature plasma, *Radio Sci.*, 52(11), 1432–1448, doi:10.1002/2017RS006294.

Glassmeier, K.-H., and F. M. Neubauer (1993), Low-frequency electromagnetic plasma waves at comet p/grigg-skjellerup: Overview and spectral characteristics, *J. Geophys. Res.: Space Phys.*, 98(A12), 20,921–20,935, doi:10.1029/93JA02583.

Glassmeier, K.-H., A. J. Coates, M. H. Acuña, M. L. Goldstein, A. D. Johnstone, F. M. Neubauer, and H. Rème (1989), Spectral characteristics of low-frequency plasma turbulence upstream of Comet P/Halley, *J. Geophys. Res.: Space Phys.*, 94(A1), 37–48, doi:10.1029/JA094iA01p00037.

Glassmeier, K.-H., H. Boehnhardt, D. Koschny, E. Kührt, and I. Richter (2007), The Rosetta Mission: Flying towards the origin of the solar system, *Space Sci. Rev.*, 128(1-4), 1–21, doi:10.1007/s11214-006-9140-8.

Goetz, C., C. Koenders, I. Richter, K. Altwegg, J. Burch, C. Carr, et al. (2016a), First detection of a diamagnetic cavity at comet 67P/Churyumov-Gerasimenko, *Astron. Astrophys.*, 588, A24, doi:10.1051/0004-6361/201527728.

Goetz, C., C. Koenders, K. C. Hansen, J. Burch, C. Carr, A. Eriksson, et al. (2016b), Structure and evolution of the diamagnetic cavity at comet 67P/Churyumov-Gerasimenko, *Mon. Not. R. Astron. Soc.*, 462, S459–S467, doi:10.1093/mnras/stw3148.

Goetz, C., M. Volwerk, I. Richter, and K.-H. Glassmeier (2017), Evolution of the magnetic field at comet 67P/Churyumov-Gerasimenko, *Mon. Not. R. Astron. Soc.*, 469, S268–S275, doi:10.1093/mnras/stx1570.

Goetz, C., B. Tsurutani, P. Henri, M. Volwerk, E. Behar, N. J. T. Edberg, et al. (2019), Unusually high magnetic fields in the coma of 67P/Churyumov-Gerasimenko during its high activity phase, *Astron. Astrophys.* 630, A38, doi:10.1051/0004-6361/201833544.

Goldstein, R., J. L. Burch, P. Mokashi, K. Mandt, C. Carr, A. Eriksson, et al. (2017), Two years of solar wind and pickup ion measurements at comet 67P/Churyumov-Gerasimenko, *Mon. Not. R. Astron. Soc.*, 469(Suppl2), S262–S267, doi:10.1093/mnras/stx1571.

Grün, E., J. Agarwal, N. Altobelli, K. Altwegg, M. S. Bentley, N. Biver, et al. (2016), The 2016 Feb 19 outburst of comet 67P/CG: An ESA Rosetta multi-instrument study, *Mon. Not. R. Astron. Soc.*, 462(Suppl1), S220–S234, doi:10.1093/mnras/stw2088.

Gunell, H., H. Nilsson, M. Hamrin, A. Eriksson, E. Odelstad, R. Maggiolo, et al. (2017a), Ion acoustic waves at comet 67P/Churyumov-Gerasimenko. Observations and computations, *Astron. Astrophys.*, 600, A3, doi:10.1051/0004-6361/201629801.

Gunell, H., C. Goetz, A. Eriksson, H. Nilsson, C. Simon Wedlund, P. Henri, et al. (2017b), Plasma waves confined to the diamagnetic cavity of comet 67P/Churyumov-Gerasimenko, *Mon. Not. R. Astron. Soc*., 469(Suppl2), S84–S92, doi:10.1093/mnras/stx1134.

Gunell, H., C. Goetz, C. Simon Wedlund, J. Lindkvist, M. Hamrin, H. Nilsson, et al. (2018), The infant bow shock: a new frontier at a weak activity comet, *Astron. Astrophys.*, 619, L2.

Hajra, R., P. Henri, X. Vallières, M. Galand, K. Héritier, A. I. Eriksson, et al. (2017), Impact of a cometary outburst on its ionosphere. Rosetta Plasma Consortium observations of the outburst exhibited by comet 67P /Churyumov-Gerasimenko on 19 February 2016, *Astron. Astrophys.*, 607, A34, doi:10.1051/0004-6361/201730591.

Hajra, R., P. Henri, M. Myllys, K. L. Héritier, M. Galand, C. Simon Wedlund, et al. (2018a), Cometary plasma response to interplanetary corotating interaction regions during 2016 June–September: a quantitative study by the Rosetta Plasma Consortium, *Mon. Not. R. Astron. Soc.*, 480(4), 4544–4556, doi:10.1093/mnras/sty2166.

Hajra, R., P. Henri, X. Vallières, J. Moré, N. Gilet, G. Wattieaux, et al. (2018b), Dynamic unmagnetized plasma in the diamagnetic cavity around comet 67P/Churyumov-Gerasimenko, *Mon. Not. R. Astron. Soc.*, 475(3), 4140–4147, doi:10.1093/mnras/sty094.

Hansen, K. C., K. Altwegg, J.-J. Berthelier, A. Bieler, N. Biver, D. Bockelée-Morvan, et al. (2016), Evolution of water production of 67P/Churyumov-Gerasimenko: An empirical model and a multi-instrument study, *Mon. Not. R. Astron. Soc.*, 462, S491–S506, doi:10.1093/mnras/stw2413.

Henri, P., X. Vallières, R. Hajra, C. Goetz, I. Richter, K.-H. Glassmeier, M. Galand, et al. (2017), Diamagnetic region(s): Structure of the unmagnetised plasma around comet 67P/CG, *Mon. Not. R. Astron. Soc.*, 469(Suppl2), S372–S379, https://doi.org/10.1093/mnras/stx1540.

Heritier, K. L., P. Henri, X. Vallières, M. Galand, E. Odelstad, A. I. Eriksson, et al. (2017), Vertical structure of the

near-surface expanding ionosphere of comet 67P probed by Rosetta, *Mon. Not. Roy. Astron. Soc.*, 469, S118–S129, doi:10.1093/mnras/stx1459.

Heritier, K. L., M. Galand, P. Henri, F. L. Johansson, A. Beth, A. I. Eriksson, et al. (2018), Plasma source and loss at Comet 67P during the Rosetta mission, *Astron. Astrophys.*, 618, A77, doi:10.1051/0004-6361/201832881.

Huang, Z., G. Tóth, T. I. Gombosi, X. Jia, M. Rubin, N. Fougere, et al. (2016), Four-fluid MHD simulations of the plasma and neutral gas environment of comet 67P/Churyumov-Gerasimenko near perihelion, *J. Geophys. Res.: Space Phys.*, 121(5), 4247–4268, doi:10.1002/2015JA022333.

Johnstone, A. D., A. J. Coates, D. E. Huddleston, K. Jockers, B. Wilken, H. Borg, et al. (1993), Observations of the solar wind and cometary ions during the encounter between Giotto and Comet Grigg-Skjellerup, *Astron. Astrophys.*, 273.

Karlsson, T., A. I. Eriksson, E. Odelstad, M. André, G. Dickeli, A. Kullen, et al. (2017), Rosetta measurements of lower hybrid frequency range electric field oscillations in the plasma environment of Comet 67P, *Geophys. Res. Lett.*, 44(4), doi:10.1002/2016GL072419, 2016GL072419.

Koenders, C., K.-H. Glassmeier, I. Richter, H. Ranocha, and U. Motschmann (2015), Dynamical features and spatial structures of the plasma interaction region of 67P/Churyumov-Gerasimenko and the solar wind, *Planet. Space Sci.*, 105, 101–116, doi:https://doi.org/10.1016/j.pss.2014.11.014.

Koenders, C., C. Goetz, I. Richter, U. Motschmann, and K.-H. Glassmeier (2016a), Magnetic field pile-up and draping at intermediately active comets: results from comet 67P/Churyumov-Gerasimenko at 2.0 AU, *Mon. Not. R. Astron. Soc.*, 462, S235–S241, doi:10.1093/mnras/stw2480.

Koenders, C., Perschke, C., Goetz, C., Richter, I., Motschmann, U., and Glassmeier, K. H. (2016b), Low-frequency waves at comet 67P/Churyumov-Gerasimenko – observations compared to numerical simulations, *Astron. Astrophys.*, 594, A66, doi:10.1051/0004-6361/201628803.

Krankowsky, D., P. Lammerzahl, I. Herrwerth, J. Woweries, P. Eberhardt, U. Dolder, et al. (1986), In situ gas and ion measurements at comet Halley, *Nature*, 321, 326–329, doi:10.1038/321326a0.

Lindkvist, J., M. Hamrin, H. Gunell, H. Nilsson, C. Simon Wedlund, E. Kallio, et al. (2018), Energy conversion in cometary atmospheres. Hybrid modeling of 67P/Churyumov-Gerasimenko, *Astron. Astrophys.*, 616, A81, doi:10.1051/0004-6361/201732353.

Madanian, H., T. E. Cravens, A. Rahmati, R. Goldstein, J. Burch, A. I. Eriksson, et al. (2016), Suprathermal electrons near the nucleus of comet 67P/Churyumov-Gerasimenko at 3 AU: Model comparisons with Rosetta data, *J. Geophys. Res.: Space Phys.*, 121(6), 5815–5836, doi:10.1002/2016JA022610.

Madsen, B., C. S. Wedlund, A. Eriksson, C. Goetz, T. Karlsson, H. Gunell, et al. (2017), Extremely low-frequency waves inside the diamagnetic cavity of comet 67P/Churyumov-Gerasimenko, *Geophys. Res. Lett.*, 45(9), 3854–3864, doi:10.1029/2017GL076415.

Mandt, K. E., A. Eriksson, N. J. T. Edberg, C. Koenders, T. Broiles, S. A. Fuselier, et al. (2016), RPC observation of the development and evolution of plasma interaction boundaries at 67P/Churyumov-Gerasimenko, *Mon. Not. R. Astron. Soc.*, 462, S9–S22, doi:10.1093/mnras/stw1736.

Meier, P, K.-H. Glassmeier, and U. Motschmann (2016), Modified ion-Weibel instability as a possible source of wave activity at comet 67P/Churyumov-Gerasimenko, *Ann. Geophys.*, 34(9), 691–707, doi:10.5194/angeo-34-691-2016.

Motschmann, U., and K.-H. Glassmeier (1993), Nongyrotropic distribution of pickup ions at comet P/Grigg-Skjellerup: A possible source of wave activity, *J. Geophys. Res.: Space Phys.*, 98(A12), 20977–20983, doi:10.1029/93JA02533.

Nemeth, Z., J. Burch, C. Goetz, R. Goldstein, P. Henri, C. Koenders, et al. (2016), Charged particle signatures of the diamagnetic cavity of comet 67P/Churyumov-Gerasimenko, *Mon. Not. R. Astron. Soc.*, 462, S415–S421, doi:10.1093/mnras/stw3028.

Neubauer, F. M., K. H. Glassmeier, M. Pohl, J. Raeder, M. H. Acuna, L. F. Burlaga, et al. (1986), First results from the Giotto magnetometer experiment at comet Halley, *Nature*, 321(6067s), 352–355.

Neubauer, F. M., K. H. Glassmeier, A. J. Coates, and A. D. Johnstone (1993), Low-frequency electromagnetic plasma waves at comet P/Grigg-Skjellerup: Analysis and interpretation, *J. Geophys. Res.: Space Phys.*, 98(A12), 20937–20953, doi:10.1029/93JA02532.

Neugebauer, M. (1990), Spacecraft observations of the interaction of active comets with the solar wind, *Rev. Geophys.*, 28(2), 231–252, doi:10.1029/RG028i002p00231.

Nilsson, H., R. Lundin, K. Lundin, S. Barabash, H. Borg, O. Norberg, A. Fedorov, et al. (2007), RPC-ICA: The ion composition analyzer of the Rosetta Plasma Consortium, *Space Sci. Rev.*, 128(1-4), 671–695, doi:10.1007/s11214-006-9031-z.

Nilsson, H., G. Stenberg Wieser, E. Behar, C. S. Wedlund, H. Gunell, M. Yamauchi, et al. (2015a), Birth of a comet magnetosphere: A spring of water ions, *Science*, 347(1), aaa0571, doi:10.1126/science.aaa0571.

Nilsson, H., G. Stenberg Wieser, E. Behar, C. Simon Wedlund, E. Kallio, H. Gunell, et al. (2015b), Evolution of the ion environment of comet 67P/Churyumov-Gerasimenko. Observations between 3.6 and 2.0 AU, *Astron. Astrophys.*, 583, A20, doi:10.1051/0004-6361/201526142.

Nilsson, H., G. Stenberg Wieser, E. Behar, H. Gunell, M. Wieser, M. Galand, et al. (2017), Evolution of the ion environment of comet 67P during the Rosetta mission as seen by RPC-ICA, *Mon. Not. Roy. Astron. Soc.*, 469, S252–S261, doi:10.1093/mnras/stx1491.

Nilsson, H., H. Gunell, T. Karlsson, N. Brenning, P. Henri, C. Goetz, et al. (2018), Size of a plasma cloud matters. The polarisation electric field of a small-scale comet ionosphere, *Astron. Astrophys.*, 616, A50, doi:10.1051/0004-6361/201833199.

Odelstad, E., A. I. Eriksson, N. J. T. Edberg, F. Johansson, E. Vigren, M. André, et al. (2015), Evolution of the plasma environment of comet 67P from spacecraft potential measurements by the Rosetta Langmuir probe instrument, *Geophys. Res. Lett.*, 42(23), 10126–10134, doi:10.1002/2015GL066599.

Odelstad, E., G. Stenberg-Wieser, M. Wieser, A. I. Eriksson, H. Nilsson, and F. L. Johansson (2017), Measurements of the electrostatic potential of Rosetta at comet 67P, *Mon. Not.*

Roy. Astron. Soc., 469, S568–S581, doi:10.1093/mnras/stx2232.

Odelstad, E., A. I. Eriksson, F. L. Johansson, E. Vigren, P. Henri, N. Gilet, et al. (2018a), Ion velocity and electron temperature inside and around the diamagnetic cavity of comet 67P, *J. Geophys. Res.: Space Phys.*, 123(7), 5870–5893, doi:10.1029/2018JA025542.

Odelstad, E., A. I. Eriksson, F. L. Johansson, E. Vigren, P. Henri, N. Gilet, et al. (2018b), Ion velocity and electron temperature inside and around the diamagnetic cavity of comet 67P, *J. Geophys. Res.: Space Phys.*, 23, 5870–5893, https://doi.org/10.1029/2018JA025542.

Ogino, T., R. J. Walker, and M. Ashour-Abdalla (1988), A three-dimensional MHD simulation of the interaction of the solar wind with comet Halley, *J. Geophys. Res.: Space Phys.*, 93(A9), 9568–9576, doi:10.1029/JA093iA09p09568.

Rème, H. (1991), Cometary plasma observations between the shock and the contact surface. In A. Johnstone (Ed.), *Cometary plasma processes*, *Geophysical Monograph Series* (Vol. 61, pp. 87–105). American Geophysical Union, Washingtonm DC, doi:10.1029/GM061p0087.

Richter, I., C. Koenders, H.-U. Auster, D. Frühauff, C. Götz, P. Heinisch, et al. (2015), Observation of a new type of low-frequency waves at comet 67P/Churyumov-Gerasimenko, *Ann. Geophys.*, 33, 1031–1036, doi:10.5194/angeo-33-1031-2015.

Simon Wedlund, C., E. Kallio, M. Alho, H. Nilsson, G. Stenberg Wieser, H. Gunell, et al. (2016), The atmosphere of comet 67P/Churyumov-Gerasimenko diagnosed by charge-exchanged solar wind alpha particles, *Astron. Astrophys.*, 587, A154, doi:10.1051/0004-6361/201527532.

Simon Wedlund, C., M. Alho, G. Gronoff, E. Kallio, H. Gunell, H. Nilsson, et al. (2017), Hybrid modelling of cometary plasma environments. I. Impact of photoionisation, charge exchange, and electron ionisation on bow shock and cometopause at 67P/Churyumov-Gerasimenko, *Astron. Astrophys.*, 604, A73, doi:10.1051/0004-6361/201730514.

Simon Wedlund, C., D. Bodewits, M. Alho, E. Behar, G. Gronoff, H. Gunell, et al. (2019a), Solar wind charge exchange in cometary atmospheres. I. Charge-exchange and ionisation cross sections for He and H particles in H_2O, *Astron. Astrophys.*, 630, A35, https://doi.org/10.1051/0004-6361/201834848.

Simon Wedlund, C., E. Behar, E. Kallio, H. Nilsson, M. Alho, H. Gunell, et al. (2019b), Solar wind charge exchange in cometary atmospheres. II. Analytical formulation, *Solar wind charge exchange in cometary atmospheres. II. Analytical model, Astron. Astrophys.*, 630, doi:10.1051/0004-6361/201834874.

Simon Wedlund, C., E. Behar, H. Nilsson, M. Alho, E. Kallio, H. Gunell, et al. (2019c), Solar wind charge exchange in cometary atmospheres. III. A Results from the Rosetta mission to comet 67P/Churyumov–Gerasimenko, *Astron. Astrophys.*, 630, A37.

Stenberg Wieser, G., E. Odelstad, H. Nilsson, and M. Wieser (2017), Investigating short time-scale variations in cometary ions around comet 67P, *Mon. Not. R. Astron. Soc.*, p. this issue.

Szegö, K., K.-H. Glassmeier, R. Bingham, A. Bogdanov, C. Fischer, G. Haerendel, et al. (2000), Physics of mass loaded plasmas, *Space Sci. Rev.*, 94, 429–671.

Taylor, M. G. G. T., N. Altobelli, B. J. Buratti, and M. Choukroun (2017), The Rosetta mission orbiter science overview: the comet phase, *Philos. Trans. R. Soc., A*, 375(2097), doi:10.1098/rsta.2016.0262.

Trotignon, J. G., J. L. Michau, D. Lagoutte, M. Chabassière, G. Chalumeau, F. Colin, et al. (2007), RPC-MIP: the Mutual Impedance Probe of the Rosetta Plasma Consortium, *Space Sci. Rev.*, 128, 713–728, doi:10.1007/s11214-006-9005-1.

Vigren, E., and A. Eriksson (2017), A 1D model of radial ion motion interrupted by ion–neutral interactions in a cometary coma, *Astron. J.*, 153(4), 150.

Vigren, E., and M. Galand (2013), Predictions of ion production rates and ion number densities within the diamagnetic cavity of comet 67P/Churyumov-Gerasimenko at perihelion, *Astrophys. J.*, 772(1), 33.

Volwerk, M., I. Richter, B. Tsurutani, C. Götz, K. Altwegg, T. Broiles, et al. (2016), Mass-loading, pile-up, and mirror-mode waves at comet 67P/Churyumov-Gerasimenko, *Ann. Geophys.*, 34(1), 1–15, doi:10.5194/angeo-34-1-2016.

Volwerk, M., G. H. Jones, T. Broiles, J. Burch, C. Carr, A. J. Coates, et al. (2017), Current sheets in comet 67P/Churyumov-Gerasimenko's coma, *J. Geophys. Res.: Space Phys.*, 122(3), 3308–3321, doi:10.1002/2017JA023861.

Volwerk, M., C. Goetz, I. Richter, M. Delva, K. Ostaszewski, K. Schwingenschuh, and K.-H. Glassmeier (2018), A tail like no other. The RPC-MAG view of Rosetta's tail excursion at comet 67P/Churyumov-Gerasimenko, *Astron. Astrophys.*, 614, A10, doi:10.1051/0004-6361/201732198.

Young, D. T., F. J. Crary, J. E. Nordholt, F. Bagenal, D. Boice, J. L. Burch, et al. (2004), Solar wind interactions with Comet 19P/Borrelly, *Icarus*, 167, 80–88, doi:10.1016/j.icarus.2003.09.011.